Revision 1

Protocaseyite, a new decavanadate mineral containing a $[Al_4(OH)_6(H_2O)_{12}]^{6+}$ linear tetramer, a novel isopolycation

Anthony R. Kampf[1,*], Mark A. Cooper[2], John M. Hughes[3], Chi Ma[4], William H. Casey[5], Frank C. Hawthorne[2], and Joe Marty[6]

[1]Mineral Sciences Department, Natural History Museum of Los Angeles County, Los Angeles, CA 90007, U.S.A.
[2]Department of Geological Sciences, University of Manitoba, Winnipeg, Manitoba, R3T 2N2, Canada
[3]Department of Geology, University of Vermont, Burlington, VT 05405, U.S.A.
[4]Division of Geological and Planetary Sciences, California Institute of Technology, Pasadena, California 91125, U.S.A.
[5]Department of Chemistry, Department of Earth and Planetary Sciences, University of California at Davis, Davis, CA 95616, U.S.A.
[6]5199 E. Silver Oak Road, Salt Lake City, UT 84108, U.S.A.
*Corresponding author: akampf@nhm.org

ABSTRACT

Protocaseyite, $[Al_4(OH)_6(H_2O)_{12}][V_{10}O_{28}]\cdot 8H_2O$, is a new mineral (IMA 2020-090) occurring in low-temperature, post-mining, secondary mineral assemblages at the Burro mine, Slick Rock district, San Miguel County, Colorado, USA. Crystals of protocaseyite are saffron-yellow, thick blades, with pale orange-yellow streak, vitreous luster, brittle tenacity, curved fracture, two very good cleavages, a Mohs hardness of 2, and a density of 2.45(2) g/cm^3. The optical properties of protocaseyite could be only partly determined: biaxial with $\alpha = 1.755(5)$, $\beta < 1.80$, $\gamma > 1.80$ (white light); pleochroic with *X* and *Y* yellow, *Z* orange ($X \approx Y < Z$). Electron-probe microanalysis and crystal-structure solution and refinement provided the empirical formula $[(Al_{3.89}Mg_{0.11}Ca_{0.02})_{\Sigma 4.02}(OH)_6(H_2O)_{12}][H_{0.06}V_{10}O_{28}]\cdot 8H_2O$. Protocaseyite is triclinic, *P*-1, $a = 9.435(2)$, $b = 10.742(3)$, $c = 11.205(3)$ Å, $\alpha = 75.395(7)$, $\beta = 71.057(10)$, $\gamma = 81.286(6)°$, $V = 1036.4(5)$ Å^3, and $Z = 1$. The crystal structure ($R_1 = 0.026$ for 4032 $I_o > 2\sigma I$ reflections) contains both the $[V_{10}O_{28}]^{6-}$ decavanadate polyoxoanion and a novel $[Al_4(OH)_6(H_2O)_{12}]^{6+}$ polyoxocation.

Keywords: protocaseyite; new mineral; polyoxometalate; crystal structure; Burro mine, San Miguel County, Colorado, USA

INTRODUCTION

Low-temperature near-surface environments, particularly those containing highly charged metal cations, have the potential to form polyoxometalate ions. In recent years, extensive work on low-temperature phases associated with surficial alteration has led to the discovery of many minerals containing large polyoxometalate ions. Deposits in the Uravan Mineral Belt of Colorado and Utah have been a rich source of uranium and vanadium ores for more than a century. They have also been a rich source of post-mining secondary vanadium minerals that typically form in mine tunnels. The most common of these are minerals containing the decavanadate $[V_{10}O_{28}]^{6-}$ isopolyanion, or its protonated or mixed-valence variants. Sherwoodite, from the Peanut mine in Montrose County, Colorado (Thompson et al. 1958), was the first mineral confirmed to contain a heteropolyanion, the $(AlV^{4+,5+}_{14}O_{40})^{n-}$ vanadoaluminate anion (Evans and Konnert 1978), which is structurally similar to the decavanadate anion. In recent years, new minerals containing variants of the Keggin heteropolyanion (Kondinski and Parac-Vogt 2018) have also been discovered in mines in the Uravan Mineral Belt. These include kegginite, $Pb_3Ca_3[AsV_{12}O_{40}(VO)]\cdot 20H_2O$, from the Packrat mine (Mesa County, Colorado) containing a mono-capped Keggin ε-isomer (Kampf et al. 2017a), and bicapite, $KNa_2Mg_2(H_2PV^{5+}_{14}O_{42})\cdot 25H_2O$, from the Pickett Corral mine (Montrose County, Colorado) containing a bi-capped Keggin α-isomer (Kampf et al. 2019a). The Packrat mine has also yielded several new minerals containing a novel $[As^{3+}V^{4+,5+}_{12}As^{5+}_{6}O_{51}]^{n-}$ heteropolyanion (Kampf et al. 2016).

The name protocaseyite links the mineral to caseyite (Kampf et al. 2020a), which contains, as a core cation, a member of the class of aluminum clusters that have sheets of Al^{3+} linked by μ_3-OH bridges and that are referred to colloquially as 'flatimers'. This term

distinguishes the sheet clusters from the more common Keggin-based structures of aluminum polyoxocations. These flatimers have only recently been discovered in nature and, in particular, in the vanadoaluminate flatimer, ideally $[(V^{5+}O_2)Al_{10}(OH)_{20}(H_2O)_{18}]^{11+}$, in the structure of caseyite. The new mineral protocaseyite, described in this paper, contains the $[Al_4(OH)_6(H_2O)_{12}]^{6+}$ tetramer, which has no μ_3-OH bridges. We refer to it as a 'flatimer', in any case, because it is the smallest cluster that can be made stable by coordination by hydrogen bonding to a decametalate anion. We thus speculate that the tetramer in protocaseyite is genetically related to caseyite and other polynuclear Group 13 cations that could be coordinated by the decavanadate anions.

The new mineral and name have been approved by the Commission on New Minerals, Nomenclature and Classification of the International Mineralogical Association (IMA2020–090). Three cotype specimens, all micromounts, are deposited in the collections of the Natural History Museum of Los Angeles County, Los Angeles, California, USA; catalogue numbers 75191, 75192 and 75193.

OCCURRENCE

Protocaseyite was found underground at the Burro mine, Slick Rock district, San Miguel County, Colorado, USA (38.04507, –108.88972). The Burro mine is the type locality for ammoniolasalite (Kampf et al. 2018a), ammoniomatesiusite (Kampf et al. 2019b), ammoniozippeite (Kampf et al. 2018b), burroite (Kampf et al. 2017b), caseyite (Kampf et al. 2020a), metamunirite (Evans, 1991), metauroxite (Kampf et al. 2020b), okieite (Kampf et al. 2020c), and uroxite (Kampf et al. 2020b). The mine is near the southern end of the Uravan Mineral Belt in which uranium and vanadium minerals occur together in bedded or roll-front deposits in the sandstone of the Salt Wash member of the Jurassic Morrison Formation (Carter

and Gualtieri 1965; Shawe 2011). The U and V ore mineralization formed where solutions rich in U and V encountered pockets of strongly reducing solutions that had developed around accumulations of carbonaceous plant material.

The specimens of the new mineral were collected by one of the authors (JM). The mineral is rare. It occurs with ammoniozippeite, gypsum, postite (Kampf et al. 2012) and another potentially new Al vanadate on montroseite- and corvusite-bearing sandstone. Protocaseyite forms by oxidation of montroseite-corvusite assemblages in a moist environment. Mining operations have exposed both unoxidized and oxidized phases. Under ambient temperatures and generally oxidizing near-surface conditions, water reacts with pyrite to form aqueous solutions of relatively low pH. The various secondary vanadate phases that form depend on ambient Eh-pH conditions and the presence of other cations (*e.g.*, NH_4^+, Na^+, Ca^{2+}, Mg^{2+}, Mn^{2+}, Pb^{2+}).

PHYSICAL AND OPTICAL PROPERTIES

Crystals of protocaseyite are thick blades up to 0.2 mm in length, commonly occurring in subparallel intergrowths and divergent groups (Fig. 1). The blades are elongated on [10-1] and flattened on {111}. The only crystal form that could be determined with certainty is {111}; other likely forms are {010}, {-111}, {11-1} and {1-21} (Fig. 2). The color of the mineral is saffron yellow, its streak is pale orange yellow, and it has vitreous luster. The mineral is non-fluorescent in long- and short-wave ultraviolet light. The crystals are brittle, with curved fracture, and have a Mohs hardness of 2 based on scratch tests. There are probably two very good cleavages, one on {111} and one along the length of the blades and at an angle to the {111} face (possibly on {010}). The density measured by floatation in a mixture of methylene iodide and toluene is 2.45(2) g/cm^3. The calculated density is 2.448 g/cm^3 based on the empirical formula using the

This is the peer-reviewed, final accepted version for American Mineralogist, published by the Mineralogical Society of America.
The published version is subject to change. Cite as Authors (Year) Title. American Mineralogist, in press.
DOI: https://doi.org/10.2138/am-2022-8059. http://www.minsocam.org/

single-crystal cell parameters. At room temperature, the mineral is insoluble in H_2O, but is easily soluble in dilute HCl.

The small size and intergrown nature of crystals, the relatively high indices of refraction, and the extreme dispersion complicated the determination of optical properties. Conoscopic observation was inconclusive and numerous attempts to obtain extinction measurements failed because of the extreme dispersion. The mineral is obviously biaxial, but the sign could not be determined and $2V$ could not be measured. The only index of refraction that could be determined (in white light) unambiguously was $\alpha = 1.755(5)$. The highest index of refraction measured on flat-lying blades was 1.800(5) and this is clearly intermediate between β and γ; therefore, $\beta < 1.80$ and $\gamma > 1.80$. Assuming $n_{av} = 1.78$, the Gladstone-Dale compatibility $1 - (K_p/K_c)$ is 0.011 for both the empirical and ideal formulas, in the range of superior compatibility (Mandarino 2007). The pleochroism varies from yellow to orange, with only one optical direction (presumed to be Z) appearing orange; therefore, X and Y yellow, Z orange; $X \approx Y < Z$. The optical orientation could not be determined.

CHEMICAL ANALYSIS

Analyses (7 points) were done at Caltech on a JEOL 8200 electron microprobe in WDS mode. Analytical conditions were 15 kV accelerating voltage, 5 nA beam current and 2 μm defocused beam diameter. During vacuum deposition of the conductive carbon coat required for EPMA, protocaseyite clearly suffered loss of much of the weakly held H_2O; no further loss was detected during EPMA. The very large H_2O loss resulted in much higher concentrations of the remaining constituents than are to be expected for the fully hydrated phase; therefore, the other analyzed constituents have been normalized to provide a total of 100% when combined with the

H_2O content derived from crystal-structure analysis. Analytical data are given in Table 1. The empirical formula is $[(Al_{3.89}Mg_{0.11}Ca_{0.02})_{\Sigma 4.02}(OH)_6(H_2O)_{12}][H_{0.06}V_{10}O_{28}]\cdot 8H_2O$ based on 54 O *apfu*. The end-member formula is $[Al_4(OH)_6(H_2O)_{12}][V_{10}O_{28}]\cdot 8H_2O$, which requires Al_2O_3 13.35, V_2O_5 59.53, H_2O 27.12, total 100 wt%.

X-RAY CRYSTALLOGRAPHY AND STRUCTURE DETERMINATION

The X-ray powder diffraction (PXRD) pattern was recorded at the Natural History Museum of Los Angeles County on a Rigaku R-Axis Rapid II microdiffractometer equipped with a curved imaging plate and monochromatized Mo$K\alpha$ radiation. A Gandolfi-like motion on the φ and ω axes was used to randomize the orientation of the sample. Observed *d*-values and intensities were derived by profile fitting using JADE Pro software (Materials Data, Inc.). Data (in Å for Mo$K\alpha$) are given in Supplemental[1] Table S1.

Single-crystal X-ray studies were done at the University of Manitoba on a Bruker D8 three-circle diffractometer equipped with a rotating-anode generator (Mo*K*a), multilayer optics, and an APEX-II detector. Structure data were collected on a crystal of protocaseyite from the holotype specimen. Satellite diffraction spots were observed, suggesting a slightly offset additional crystal domain. A second domain (37 % relative volume) rotated 2.8° from the primary domain was identified using CELL_NOW (Sheldrick 2008) and the diffraction data were integrated using orientation matrices from both domains. The multi-component data were processed using TWINABS (Sheldrick 2012) such that only reflections belonging to the primary component were retained (overlapping intensity from the satellite component was subtracted). The unit-cell dimensions were obtained by least-squares refinement of 4070 reflections with $I > 10\sigma I$.

155 The structure was solved by direct methods using SHELXS-2013 and the structure was
156 refined using SHELXL-2016 (Sheldrick 2015). All non-hydrogen atoms were located and refined
157 with anisotropic-displacement parameters and full occupancies. All hydrogen-atom sites were
158 located by difference-Fourier. Data collection and refinement details are given in Table 2, atom
159 coordinates and displacement parameters in Supplemental Table S2, cation-anion bond distances
160 in Table 3, hydrogen bonds in Table 4 and a bond-valence analysis in Table 5.
161

162 ## DESCRIPTION AND DISCUSSION OF THE STRUCTURE

163 ### The $[V_{10}O_{28}]^{6-}$ decavanadate unit

164 The $[V_{10}O_{28}]^{6-}$ decavanadate unit is shown in ball-and-stick and polyhedral
165 representations in Figure 3. The outer surface of the polyanion consists of 26 O atoms (O1
166 through O13) that are all bond-valence deficient (range = 1.62 – 1.90 vu) from the V^{5+} cation
167 contributions alone (Table 5). Eight near-planar anion surfaces define the polyanion's exterior
168 and collectively have maximal 2/*m* 2/*m* 2/*m* point-group symmetry. Four large anion surfaces,
169 each containing nine anions in a hexagonal pattern, form one prism; another prism consists of
170 four smaller triangular shaped faces, each containing six anions (Fig. 3b). For protocaseyite, the
171 point group symmetry of the decavanadate polyanion is –1, and symmetry equivalent anion faces
172 occur in pairs on opposite sides of the polyanion (the two symmetrically distinct larger anion
173 faces have their anions labelled in Figure 3b).
174

175 ### The $[Al_4(OH)_6(H_2O)_{12}]^{6+}$ flatimer

176 The $[Al_4(OH)_6(H_2O)_{12}]^{6+}$ moiety, which we refer to as a "flatimer", is an aluminum
177 polyoxocation consisting of a single layer of edge-sharing octahedra. It is shown in plan view and

178 also rotated 90° about its long axis in Figures 4a, b. A "flatimer" is a small, approximately two-
179 dimensional aluminum polyoxocation and the term distinguishes such arrangements from higher-
180 symmetry Keggin-like ions like the more familiar $[AlO_4Al_{12}(OH)_{24}(H_2O)_{12}]^{7+}$ ion. All anions (O
181 sites) are either OH groups (shared along Al–Al edges) or H_2O groups, and the Al-flatimer in
182 protocaseyite can be described as a corrugated unit of octahedra with flat top and bottom, and
183 fully decorated by H atoms. To better highlight the anion configuration of this unit, only anions
184 are drawn and connected (in plan view) in Figure 4c. Like the $[V_{10}O_{28}]$ decavanadate unit, the Al-
185 flatimer also has –1 symmetry with the center of symmetry located at its core. The Al-flatimer
186 has two symmetrically distinct planar surfaces of anions with O_{donor}–H bonds projecting from
187 both surfaces at high angles. The first is the top (or bottom) surface of the flatimer containing six
188 anions bonded to the six H atoms (H1, H2, H3, H5, H6, H9), and the second is located on the side
189 of the flatimer and contains five anions in a ring, with four of the five anions having H atoms
190 (H3, H4, H10, H14) with their O_{donor}–H bonds at a high angle to the anion surface (Fig. 4c). The
191 hexagonal pattern of the six H atoms on the top surface is a match for six anions on one of the
192 large flat anion surfaces (centered by O13) of the decavanadate, and the resulting H-bond
193 arrangement is shown in Figure 5a, b. The rhombic-shaped pattern of H atoms on the side of the
194 Al-flatimer is also a match to the anion configuration on the other large flat anion surface
195 (centered by O12) of the decavanadate, and the resulting H-bond arrangement is shown in Figure
196 5a, c.
197
198 **Linkage of the decavanadate unit and the Al-flatimer**
199 The protocaseyite structure is a layered hydrated salt. The structure consists of alternating
200 $[V_{10}O_{28}]^{6-}$ decavanadate polyanions and $[Al_4(OH)_6(H_2O)_{12}]^{6+}$ flatimers packed in a rhombic

pattern, with larger-area anion surfaces perpendicular to the plane of the pattern (Fig. 6). The decavanadate and Al-flatimer units link via strong H-bonding: the anion surfaces of the decavanadate, centered on the O13 anion, accept strong H-bonds along [111] from the upper and lower protonated surfaces of the Al-flatimer (Fig. 6); the other two surfaces of each decavanadate-anion, centered on the O12 anion, H-bond to the protonated side of the Al-flatimer along 1-11] (Fig. 6). The layer in Figure 6 links to the layers adjacent along [111] via H-bonding from interstitial (H_2O) groups (Fig. 7) that links the small decavanadate surfaces (the two sloping triangular anion faces in Figure 3b) with the ends of the Al-flatimers. Thus each $[V_{10}O_{28}]^{6-}$ decavanadate unit is surrounded by six $[Al_4(OH)_6(H_2O)_{12}]^{6+}$ flatimers, and each $[Al_4(OH)_6(H_2O)_{12}]^{6+}$ flatimer is surrounded by six $[V_{10}O_{28}]^{6-}$ decavanadate units.

Protocaseyite has a well-ordered atomic arrangement that was refined from sharp high-quality X-ray diffraction data. This is a first for a naturally occurring solid containing an extended Al-flatimer. Caseyite was the first mineral found to contain an extended Al-flatimer; however, caseyite is plagued by structural disorder that is accompanied by extensive chemical variability among its interstitial constituents (Kampf et al. 2020a). As Al-flatimers have been postulated to be important building blocks for the formation of many minerals and to occur extensively in the natural environment, the recent discovery of protocaseyite and caseyite offer important insight toward the occurrence of natural Al-flatimers in minerals. Two questions arise:

(1) Why do Al-flatimers combine with the decavanadate polyanion in minerals?

(2) Why does protocaseyite occur as extraordinarily well-ordered crystals, whereas compounds bearing tridecamer-like Al-flatimers tend to form poor crystals, if they are crystalline at all?

The following observations on the structure of protocaseyite may help to address these questions:

(1) The $[V_{10}O_{28}]^{6-}$ decavanadate polyanion has a surface of bond-valence-deficient anions that are ideal H-bond acceptors. The entire surface of an Al-flatimer is decorated by H-atoms (either as OH groups along shared Al–Al edges, or as H_2O groups). The O_{donor} anions all receive incident bond-valence from the constituent Al^{3+} ions in excess of that required to accord with the valence-sum rule assuming an O_{donor}–H of 1 vu, and hence the constituent H-atoms will form H-bonds with adjacent potential $O_{acceptor}$ anions.

(2) The decavanadate polyanion and Al-flatimers have matching flat anion surfaces with stereochemistries suitable for the formation of linking H-bonds.

(3) If the decavanadate polyanion(s) and Al-flatimers are stable and coexist in solution, the properties described in (1) and (2) suggest that they may crystallize by condensation involving the formation of linking H-bonds if the specific Al-flatimer provides a stereochemical match for the decavanadate polyanion. The well-ordered protocaseyite structure, with a simple 1:1 stoichiometry of polyanion and polycation constituents and minimal additional interstitial constituents, may represent one of the simplest and most compact decavanadate – Al-flatimer combinations to occur in crystalline form.

DECAVANADATE BOND-VALENCE ANOMALY

Reliable well-defined H positions were recovered for the (OH) and (H_2O) groups in protocaseyite from the difference-Fourier map, and the refined positions conform to well-ordered H sites exhibiting usual H-bond geometries (Table 4). The proposed bond-valence distribution among O_{donor} and $O_{acceptor}$ anions from these H positions yields bond-valence sums from 1.91 to 2.15 vu for 25 of the 27 anions, values that accord well with the valence-sum rule (Brown 2016), and noticeably low bond-valence sums of 1.77 and 1.79 vu for the O3 and O4 anions respectively

(Table 5). These O3 and O4 anions are [1]-coordinated decavanadate surface anions that form strong vanadyl bonds, and do not accept any additional bonds from interstitial constituents. Are these low bond valences significant? How do these V4–O3 and V5–O4 vanadyl bond lengths compare to other vanadyl bonds in similar decavanadate mineral structures? Are there other decavanadate mineral structures possessing similar "naked" decavanadate surface anions that do not form any additional bonds to neighboring interstitial constituents? In recent years, the number of decavanadate mineral structures has steadily increased, and eleven of these structures (including protocaseyite) were compared to address the above questions in relation to the apparent bond-valence anomaly in protocaseyite. The selection criteria focused on well-refined structures (R values < 4%) containing precise atomic positions for all atoms (i.e. well-ordered with all H positions reliably located). Cooper et al. (2019) previously noted that highly accurate bond valences can be obtained from reliable V^{5+}–O bond lengths using the bond-valence equation of Brown and Altermatt (1985). For the eleven decavanadates compared here, the calculated bond-valence sums for all V sites ranges from 4.94 – 5.14 vu, and are close to the postulated V^{5+} charge. We can infer that the complimentary bond valences at the coordinating O sites are accurate as well, and the bond-valence sums of 1.77 and 1.79 vu for the O3 and O4 anions from the V^{5+} contribution alone in protocaseyite are a major departure from the valence-sum rule. Within a given $[V_{10}O_{28}]^{6-}$ polyanion, there are eight surface anions that each receive a single vanadyl bond (Fig. 8), and for the eleven structures investigated there are 88 individual vanadyl bonds displayed on a bar graph in Figure 9. The maximum in the distribution occurs in the range ~1.60 – 1.61 Å, and the V4–O3 and V5–O4 distances of 1.5910 and 1.5871 Å in protocaseyite are distinctly short, in accord with the lack of interstitial bonds to these anions. A typical vanadyl bond of 1.606 Å would result in a bond-valence deficiency of ~0.3 vu, whereas the shorter V4–

O3 and V5–O4 distances in protocaseyite help alleviate the deficiency somewhat (i.e. reduce it to ~0.2 vu). The shortest $^{[6]}V^{5+}$-O bond observed in inorganic crystals is 1.554 Å (Gagné and Hawthorne 2020), indicating that the values of ~1.59 Å in protocaseyite may represent a near limit of bond-length distortion for the V^{5+} polyhedra involved, where any further shortening of the vanadyl bond becomes disruptive to overall bonding within the polyanion. The eight vanadyl O atoms on a given decavanadate polyanion are the most bond-valence deficient surface anions (typically ~0.3 vu deficiency) and they are also the furthest away from the central core of the polyanion. As a result, they are ideally placed to accept additional bonds from interstitial constituents. The fact that four of these eight vanadyl oxygens on the surface of the protocaseyite decavanadate polyanion do not receive any additional bonding from interstitial constituents is quite remarkable. Of all eleven structures investigated, only one other structure, namely postite (Kampf et al. 2012), contains a similar [1]-coordinated vanadyl oxygen; postite is also the only other decavanadate that also contains an interstitial flatimer, the $[Al_2(OH)_2(H_2O)_8]^{4+}$ polycation. The [1]-coordinated vanadyl oxygen in postite is at the O11 site, and the V5–O11 distance of 1.599 Å is a relatively short vanadyl distance. The [1]-coordinated vanadyl O atoms in both protocaseyite and postite are similarly situated on the equatorial girdle of the polyanion (Fig. 8). Both protocaseyite and postite have short distances between the flat anion surfaces of decavanadate polyanions and flat aluminate-hydrate polycations, which are bridged by H bonds. In turn, this may lead to relatively inaccessible *dead zones* near the fringes of these zones of H bonds, where the ability of other interstitial components to bond to some decavanadate surface anions (i.e. outermost vanadyl O atoms) is sterically inhibited. More equant interstitial constituents [e.g. $Na(H_2O)_6$ clusters or small (H_2O) groups] are more suited to provide a more complete distribution of weak bonding to all decavanadate surface anions without major steric

interference. Although only a few structures with well-behaved decavanadate – flatimer units are known, the interaction of these two types of unit apparently leads to undersaturated surface anions on the decavanadate polyanion. With a much larger $[V^{5+}O_2Al_{10}(OH)_{20}(H_2O)_{18}]^{11+}$ flatimer, caseyite invokes a novel mechanism by which it alters the bonding landscape at the periphery of the flatimer and may help to prevent a local dead zone from occurring via inversion of the steric argument: adding a $V^{5+}O_2(OH)_4$ octahedron with two outer vanadyl O atoms onto the margin of the flatimer removes any sterically interfering H atoms projecting outward from an H_2O group and allowing other interstitial constituents to bond to under-bonded anions (Kampf et al. 2020a).

IMPLICATIONS

Aluminum is the third most abundant element (after oxygen and silicon) in the Earth's crust. Although clay minerals generally maintain low Al concentrations in surface waters, the solubilities can become high in acidic solutions, such as those found near exposed ore deposits. Generally, millimolar concentrations of total dissolved aluminum are required for formation of multimeric ions like the $[AlO_4Al_{12}(OH)_{24}(H_2O)_{12}]^{7+}$, and these may actually be metastable relative to monomer ions and solids.

It is difficult to prove unequivocally that an oxide ion cluster found in a mineral previously existed separately as an ion in the precipitating solution. Such proof generally requires isotope-tracing experiments or dynamic spectroscopy. Clusters in a mineral could polymerize at the interface during mineral growth and have no existence separately in solution. In the opposite extreme, isotope-tracing experiments have shown that large cluster ions of inert metals, like Group V and VI polyoxometalates, clearly form minerals when rates of ligand exchange are much slower than rates of mineral growth (see Spiccia and Casey 2006). Even aquated monomer

316 ions form solids as intact solvated ions when the rates of ligand exchanges are much slower than
317 the rates of mineral growth. Such would be found, for example, for $[Rh(H_2O)_6]^{3+}$ ions where Rh-
318 bonded waters of hydration have an average lifetime of two years in the inner-coordination
319 sphere of the metal (Richens 1997). The metal-hydroxide solid $Rh(H_2O)_3(OH)_3$ forms
320 instantaneously when the ion is thrice deprotonated, but the inner-sphere waters never move out
321 of their positions bonded to the Rh^{3+} (see Spiccia and Marty 1986; Crimp and Spiccia 1995;
322 Spiccia 2004).

323 However, proving this point is particularly difficult for metal cations like Al^{3+}, where the
324 rates of ligand exchange are on the same time scale, or faster than, rates of mineral growth. Rates
325 of ligand substitution at Al^{3+} centers are seconds to microseconds, and are particularly fast if the
326 metal is partly hydrolyzed (Casey 2005). Thus, it is completely possible that the flatimers
327 polymerized at the growing mineral interface and have no separate lifetime as ions in solution.
328 Aluminum nanoclusters are rarely found as isolated entities in minerals. A noteworthy
329 counterexample is the α-Al_{13} Keggin cluster that forms part of the framework structure of zunyite
330 (Louisnathan and Gibbs 1972; Baur and Ohta 1982).

331 The core cation in caseyite has a tridecamer structure that is well known from synthesis
332 (Wang et al. 2011; Gatlin et al. 2008) and is referred to as a 'flatimer' to distinguish it from
333 Keggin structures. The novel $[Al_4(OH)_6(H_2O)_{12}]^{6+}$ flatimer in protocaseyite is the smallest
334 possible Al-flatimer that can assemble with $[V_{10}O_{28}]^{6-}$ polyanions in a 1:1 stoichiometry. If a
335 smaller Al-flatimer were present (e.g. $[Al_3(OH)_4(H_2O)_{10}]^{5+}$), then a 1:1 Al-flatimer-to-
336 decavanadate stoichiometry could assemble only with an additional charged (i.e. 1+) interstitial
337 constituent present. In this sense, the 'proto' designator distinguishes protocaseyite as the simple
338 proto-type structure from which all other Al-flatimer – decavanadate structures are hierarchical

derivatives. Larger Al-flatimers are expected to be identified in future studies, probably along with greater variability in additional charged interstitial constituents and possible replacement of some Al^{3+} with other highly charged cations, e.g. V^{5+} as in caseyite.

There have been many synthesis studies of polyoxometalate anions and, more rarely, polyoxometalate cations, in recent years, largely because of their potential technological uses. The occurrence of both polyoxometalate anions and polyoxometalate cations in the same crystal structure (e.g., protocaseyite, caseyite) suggests that co-crystallization of these units could provide a strategy for crystallization of synthetic phases containing species that are in aqueous solution but not readily incorporated into crystalline hydroxy-hydrated aluminates.

ACKNOWLEDGEMENTS

Two anonymous reviewers are thanked for constructive comments, which improved the manuscript. This study was funded, in part, by the John Jago Trelawney Endowment to the Mineral Sciences Department of the Natural History Museum of Los Angeles County.

REFERENCES

Baur, W.H., and Ohta, T. (1982) The Si_5O_{16} pentamer in zunyite refined and empirical relations for individual silicon–oxygen bonds. Acta Crystallographica, B38, 390–401.

Bennett, J.W., Bjorklund, J.L., Forbes, T.Z., and Mason, S.E. (2017) Systematic study of aluminum nanoclusters and anion adsorbates. Inorganic Chemistry, 56, 13014–13028.

Brown, I.D. (2016) The Chemical Bond in Inorganic Chemistry. The Bond Valence Model. 2nd Edition. Oxford University Press, U.K.

Brown, I.D., and Altermatt, D. (1985) Bond-valence parameters from a systematic analysis of the inorganic crystal structure database. Acta Crystallographica, B41, 244–247.

Carter, W.D., and Gualtieri, J.L. (1965) Geology and uranium–vanadium deposits of the La Sal quadrangle, San Juan County, Utah, and Montrose County, Colorado. United States Geological Survey Professional Paper, 508.

Casey, W.H. (2005) Large aqueous aluminum-hydroxide molecules. Chemical Reviews, 106, 1–16.

Colombo, F., Baggio, R., and Kampf, A.R. (2011) The crystal structure of the elusive huemulite. The Canadian Mineralogist, 49, 849–864.

Cooper, M.A., Hawthorne, F.C., Kampf, A.R., and Hughes, J.M. (2019) Determination of V^{4+}:V^{5+} ratios in the $[V_{10}O_{28}]^{n-}$ decavanadate polyanion. The Canadian Mineralogist, 57, 235–244.

Crimp, S.J., and Spiccia, L. (1995) Characterization of three active rhodium(III) hydroxides. Australian Journal of Chemistry, 48, 557–566.

Evans, H.T., Jr. (1991) Metamunirite, a new anhydrous sodium metavanadate from San Miguel County, Colorado. Mineralogical Magazine, 55, 509–513.

Evans, Jr., H.T., and Konnert, J.A. (1978) The crystal chemistry of sherwoodite, a calcium 14-vanadoaluminate heteropoly complex. American Mineralogist, 63, 863–868.

Gagné, O.C., and Hawthorne, F.C (2015) Comprehensive derivation of bond-valence parameters for ion pairs involving oxygen. Acta Crystallographica, B71, 562–578.

Gatlin, J.T., Mensinger, Z.L., Zakharov, L.N., MacInnes, D., and Johnson, D. W. (2008) Facile synthesis of the tridecameric Al_{13} nanocluster $Al_{13}(\mu_3\text{-}OH)_6(\mu\text{-}OH)_{18}(H_2O)_{24}\ (NO_3)_{15}$. Inorganic Chemistry, 47, 1267–1269.

Hughes, J.M., Schindler, M., Rakovan, J., and Cureton, F.E. (2002) The crystal structure of hummerite, $KMg(V_5O_{14})\bullet 8H_2O$: bonding between the $[V_{10}O_{28}]^{6-}$ structural unit and the

386 $\{K_2Mg_2(H_2O)_{16}\}^{6+}$ interstitial complex. The Canadian Mineralogist, 40, 1429–1435.

387 Hughes, J.M., Schindler, M., and Francis, C.A. (2005) The *C*2/*m* disordered structure of pascoite,

388 $Ca_3(V_{10}O_{28})\cdot 17H_2O$. The Canadian Mineralogist, 43, 1379–1386.

389 Hughes, J.M., Wise, W.S., Gunter, M.E., Morton, J.P., and Rakovan, J. (2008) Lasalite,

390 $Na_2Mg_2[V_{10}O_{28}]\cdot 20H_2O$, a new decavanadate mineral species from the Vanadium Queen

391 Mine, La Sal District, Utah: Description, atomic arrangement, and relationship to the pascoite

392 group of minerals. The Canadian Mineralogist, 46, 1365–1372.

393 Kampf, A.R., and Steele, I.M. (2008) Magnesiopascoite, a new member of the pascoite group:

394 Description and crystal structure. The Canadian Mineralogist, 46, 679–686.

395 Kampf, A.R., Hughes, J.M., Marty, J., and Nash, B. (2012) Postite,

396 $Mg(H_2O)_6Al_2(OH)_2(H_2O)_8(V_{10}O_{28})\cdot 13H_2O$, a new mineral species from the La Sal mining

397 district, Utah: Crystal structure and descriptive mineralogy. *The Canadian Mineralogist* **50**,

398 45–53.

399 Kampf, A.R., Hughes, J.M., Nash, B.P., and Marty, J. (2014a) Kokinosite,

400 $Na_2Ca_2(V_{10}O_{28})\cdot 24H_2O$, a new decavanadate mineral species from the St. Jude mine,

401 Colorado: crystal structure and descriptive mineralogy. The Canadian Mineralogist, 52, 15–

402 25.

403 Kampf, A.R., Hughes, J.M., Nash, B.P., and Marty, J. (2016a) Vanarsite, packratite, morrisonite,

404 and gatewayite: four new minerals containing the $[As^{3+}V^{4+,5+}{}_{12}As^{5+}{}_6O_{51}]$ heteropolyanion, a

405 novel polyoxometalate cluster. The Canadian Mineralogist, 54, 145–162.

406 Kampf, A.R., Hughes, J.M., Nash, B.P., Marty, J., Cooper, M.A., Hawthorne, F.C., Karpenko,

407 V.Y., Pautov, L.A., and Agakhanov, A.A. (2016b) Revision of the formulas of wernerbaurite

408 and schindlerite: Ammonium- rather than hydronium-bearing decavanadate minerals. *The*

Canadian Mineralogist **54**, 555–558.

Kampf, A.R., Hughes, J.M., Nash, B.P., and Marty, J. (2017a) Kegginite, $Pb_3Ca_3[AsV_{12}O_{40}(VO)]\cdot 20H_2O$, a new mineral with an ε-isomer of the Keggin anion. American Mineralogist, 102, 461–465.

Kampf, A.R., Nash, B.P., Marty, J., and Hughes, J.M. (2017b) Burroite, $Ca_2(NH_4)_2(V_{10}O_{28})\cdot 15H_2O$, a new decavanadate mineral from the Burro mine, San Miguel County, Colorado. The Canadian Mineralogist, 55, 473–481.

Kampf, A.R., Nash, B.P., Adams, P.M., Marty, J., and Hughes, J.M. (2018a) Ammoniolasalite, $(NH_4)_2Mg_2(H_2O)_{20}]$ $[V_{10}O_{28}]$, a new decavanadate species from the Burro mine, Slick Rock district, Colorado. The Canadian Mineralogist, 56, 859–869.

Kampf, A.R., Plášil, J., Olds, T.A., Nash, B.P., and Marty, J. (2018b) Ammoniozippeite, a new uranyl sulfate from the Blue Lizard mine, San Juan County, Utah, and the Burro mine, San Miguel County, Colorado, USA. The Canadian Mineralogist, 56, 235–245.

Kampf, A.R., Hughes, J.M., Nash, B.P., and Marty, J. (2019a) Bicapite, $KNa_2Mg_2(H_2PV^{5+}_{14}O_{42})\cdot 25H_2O$, a new mineral with a bicapped Keggin anion from the Pickett Corral mine, Montrose County, Colorado, USA. American Mineralogist, 104, 1851–1856.

Kampf, A.R., Plášil, J., Nash, B.P., and Marty, J. (2019b) Ammoniomathesiusite, a new uranyl sulfate-vanadate mineral from the Burro mine, San Miguel County, Colorado, USA. Mineralogical Magazine, 83, 115–121.

Kampf, A.R., Cooper, M.A., Hughes, J.M., Nash, B.P., Marty, J., and Hawthorne, F.C. (2020a) Caseyite, a new mineral containing a variant of the flat-Al_{13} polyoxometalate cation. American Mineralogist, 105, 123–131.

Kampf, A.R., Plášil, J., Nash, B.P., Němec, I., and Marty, J. (2020b) Uroxite and metauroxite, the first two uranyl-oxalate minerals. Mineralogical Magazine, 84, 131–141.

Kampf, A.R., Adams, P.M., Nash, B.P., Marty, J., and Hughes, J.M. (2020c) Okieite, $Mg_3[V_{10}O_{28}]\cdot 28H_2O$, a new decavanadate mineral from the Burro mine, Slick Rock mining district, San Miguel County, Colorado, USA. The Canadian Mineralogist, 58, 125–135.

Kondinski, A., and Parac-Vogt, T.N. (2018) Keggin Structure, Quō Vādis?. Frontiers in Chemistry, 6, Article 346.

Louisnathan, S.J., and Gibbs, G.V. (1972) Aluminum-silicon distribution in zunyite. American Mineralogist, 57, 1089-1108.

Mandarino, J.A. (2007) The Gladstone–Dale compatibility of minerals and its use in selecting mineral species for further study. The Canadian Mineralogist, 45, 1307–1324.

Perkins, C.K., Eitrheim, E.S., Brantly L. Fulton, B.L., Fullmer, L.B., Colla, C.A., Park, D.-H., Oliveri, A.F., Hutchison, J.E., Nyman, M., Casey, W.H., Forbes, T.Z., Johnson, D.W., and Keszler, D.A. (2017) Synthesis of aluminum hydroxide octamer by a simple dissolution method. Angewandte Chemie, 56, 10161–10162.

Richens, D.T. (1997) Chemistry of Aqua Ions. J. Wiley.

Shawe, D.R. (2011) Uranium-vanadium deposits of the Slick Rock district, Colorado. United States Geological Survey Professional Paper, 576-F.

Sheldrick, G.M. (2008) CELL_NOW, Version 2008/4; Georg-August-Universität Göttingen: Göttingen, Germany.

Sheldrick, G.M. (2012) TWINABS 2012/1. Georg-August-University Göttingen, Göttingen, Germany.

Sheldrick, G.M. (2015) Crystal Structure refinement with SHELX. Acta Crystallographica, C71,

3–8.

Spiccia, L., and Marty, W. (1986) The fate of active chromium hydroxide, $Cr(OH)_3 \cdot 3H_2O$, in aqueous suspension. Study of the chemical changes involved in its aging. Inorganic Chemistry 25, 266–271.

Spiccia, L. (2004) Homopolynuclear and heteropolynuclear Rh(III) aqua ions – a review. Inorganica Chimica Acta, 357, 2799–2817.

Spiccia, L., and Casey, W.H. (2006) Synthesis of experimental models for molecular inorganic geochemistry-A review with examples. Geochimica et Cosmochimica Acta, 71, 5590–5604.

Wang, W., Wentz, K.M., Hayes, S.E., Johnson, D.W., and Keszler, D. (2011) Synthesis of the hydroxide cluster $[Al_{13}(\mu_3\text{-}OH)_6(\mu\text{-}OH)_{18}(H_2O)_{24}]^{15+}$ from an aqueous solution. Inorganic Chemistry, 50, 4683–4685.

Endnote:

[1]Deposit item AM-21-XXXXX, Supplemental tables and CIF. Deposit items are free to all readers and found on the MSA website, via the specific issue's Table of Contents (go to http://www.minsocam.org/MSA/AmMin/TOC/2021/Xxx2021_data/ Xxx2021_data.html).

This is the peer-reviewed, final accepted version for American Mineralogist, published by the Mineralogical Society of America.
The published version is subject to change. Cite as Authors (Year) Title. American Mineralogist, in press.
DOI: https://doi.org/10.2138/am-2022-8059. http://www.minsocam.org/

FIGURE CAPTIONS

Figure 1. Protocaseyite crystals; field of view 0.4 mm across.

Figure 2. Crystal drawing of protocaseyite; clinographic projection in non-standard orientation, [10-1] vertical.

Figure 3. The $[V_{10}O_{28}]^{6-}$ decavanadate polyanion represented as: (a) ball and stick, and (b) polyhedral representations. Orange circles = V atoms; red circles = O atoms; white circles = surface anions of the two largest non-symmetrically related anion faces of the polyanion.

Figure 4. The $[Al_4(OH)_6(H_2O)_{12}]^{6+}$ flatimer: (a) plan view, (b) rotated 90°, (c) plan view containing only anions (larger red circles: top surface anions, smaller red circles: lower surface anions, black circles: H atoms), transparent yellow planes: highlight surface anions belonging to 2nd largest anion surface; blue lines with black rims connect upper / lower surface anions, blue lines: connect lower to upper anions.

Figure 5. Hydrogen bonding between: (a) upper surface O_D anions of the $[Al_4(OH)_6(H_2O)_{12}]^{6+}$ flatimer, and (b) O_A anions of the O13-centred face; and between side O_D anions of the $[Al_4(OH)_6(H_2O)_{12}]^{6+}$ flatimer to (c) O_A anions of the O12-centred face of the $[V_{10}O_{28}]^{6-}$ decavanadate polyanion. Decavanadate polyanions represented by surface anions only (yellow and red circles), with large circles as upper surface anions, polyanion surface junctures marked with orange lines containing black rims; pale yellow shaded circles = O_D and O_A anions involved in hydrogen bond coupling (green, pink dashed lines).

Figure 6. The $[V_{10}O_{28}]^{6-}$ – $[Al_4(OH)_6(H_2O)_{12}]^{6+}$ layer in protocaseyite projected down [1-21]. Hydrogen bonds are shown as red lines. The view is approximately parallel to the plane of the layer. Interstitial H_2O groups are not shown.

Figure 7. The structure of protocaseyite projected down [10-1]. The O atoms of the interstitial (H_2O) groups are shown as red circles. The outline of the unit cell is shown in green.

Figure 8. The $[V_{10}O_{28}]^{6-}$ decavanadate polyanion in protocaseyite with the "naked" O3 and O4 atoms indicated with arrows. Note that the "naked" O11 atom in postite in is the same position as the O4 atom in protocaseyite. V atoms = black circles, [1]-coordinated O atoms = red circles, [2]-coordinated O atoms = blue circles, [3]-coordinated O atoms = green circles, [6]-coordinated O atoms = yellow circles, $V–O_{vanadyl}$ bonds = thick black line, $V–O_{trans}$ bonds = thin black line, $V–O_{equatorial}$ bonds = grey shaded line.

Figure 9. The 88 vanadyl bonds for the [1]-coordinated O atoms of 11 decavanadate mineral structures: ammoniolasalite (Kampf et al. 2018a), huemulite (Colombo et al. 2011), hummerite (Hughes et al. 2002), kokinosite (Kampf et al. 2014a), lasalite (Hughes et al. 2008), magnesiopascoite (Kampf and Steele 2008), okieite (Kampf et al. 2020c), pascoite (Hughes et al. 2005), postite (Kampf et al. 2012), protocaseyite (this study), and wernerbaurite (Kampf et al. 2016b).

511 Table 1. Chemical analytical data in wt% for protocaseyite.
512

Constituent	Mean	Range	S.D.	Standard	Normalized
MgO	0.32	0.27–0.37	0.03	forsterite	0.28
CaO	0.09	0.07–0.10	0.01	anorthite	0.08
Al_2O_3	14.86	14.42–15.30	0.33	anorthite	12.98
V_2O_5	68.10	66.70–69.43	1.04	V_2O_5	59.51
H_2O*					27.15
Total					100.00

513 * Based upon the crystal structure with V = 10 and O = 54 *apfu*.
514
515

Table 2. Data collection and structure-refinement details for protocaseyite.

Diffractometer	Bruker D8 three-circle
X-ray radiation / source	Mo$K\alpha$ (λ = 0.71073 Å) / rotating anode
Temperature	293(2) K
Structural Formula	$[Al_4(OH)_6(H_2O)_{12}][V_{10}O_{28}]\cdot 8H_2O$
Space group	*P*-1
Unit cell dimensions	a = 9.435(2) Å α = 75.395(7)°.
	b = 10.742(3) Å β = 71.057(10)°.
	c = 11.205(3) Å γ = 81.286(6)°.
V	1036.4(5) Å^3
Z	1
Density (for above formula)	2.448 g cm^{-3}
Absorption coefficient	2.383 mm^{-1}
F(000)	760
Crystal size	45 × 22 × 15 μm
θ range	2.81 to 27.59°
Index ranges	$-12 \le h \le 12$, $-13 \le k \le 13$, $-14 \le l \le 14$
Reflections collected/unique	30690/4786; R_{int} = 0.0347
Reflections with $I > 2\sigma I$	4032
Completeness to θ = 27.59°	99.9%
Refinement method	Full-matrix least-squares on F^2
Parameters/restraints	377/23
GoF	1.072
Final R indices [$I > 2\sigma I$]	R_1 = 0.0254, wR_2 = 0.0689
R indices (all data)	R_1 = 0.0333, wR_2 = 0.0716
Largest diff. peak/hole	+0.64/–0.33 e A^{-3}

$R_{int} = \Sigma|F_o^2 - F_o^2(\text{mean})|/\Sigma[F_o^2]$. GoF = $S = \{\Sigma[w(F_o^2 - F_c^2)^2]/(n-p)\}^{1/2}$. $R_1 = \Sigma||F_o| - |F_c||/\Sigma|F_o|$. $wR_2 = \{\Sigma[w(F_o^2 - F_c^2)^2]/\Sigma[w(F_o^2)^2]\}^{1/2}$; $w = 1/[\sigma^2(F_o^2) + (aP)^2 + bP]$ where a is 0.0297, b is 1.2951 and P is $[2F_c^2 + \text{Max}(F_o^2, 0)]/3$.

548 Table 3. Selected bond distances (in Å) in protocaseyite.
549

V1–O5	1.6764(17)	V4–O3	1.5910(18)	Al1–OH3	1.8327(18)
V1–O6	1.7048(17)	V4–O11	1.8522(17)	Al1–OH1	1.8530(18)
V1–O12	1.9194(16)	V4–O10	1.8652(17)	Al1–OH1	1.8852(18)
V1–O13	1.9337(16)	V4–O7	1.8859(17)	Al1–OH2	1.9122(18)
V1–O14	2.1049(16)	V4–O5	2.0657(17)	Al1–OW1	1.9419(19)
V1–O14	2.1300(16)	V4–O14	2.2969(16)	Al1–OW2	1.967(2)
<V1–O>	1.912	<V4–O>	1.926	<Al1–O>	1.899
V2–O1	1.6012(17)	V5–O4	1.5871(18)	Al2–OH3	1.8221(18)
V2–O7	1.8266(17)	V5–O11	1.8492(17)	Al2–OH2	1.8564(18)
V2–O8	1.8327(17)	V5–O8	1.8637(17)	Al2–OW5	1.8972(19)
V2–O12	1.9941(16)	V5–O9	1.9098(18)	Al2–OW4	1.9013(19)
V2–O13	2.0031(16)	V5–O6	2.0326(17)	Al2–OW6	1.906(2)
V2–O14	2.2424(16)	V5–O14	2.3633(16)	Al2–OW3	1.9576(19)
<V2–O>	1.917	<V5–O>	1.934	<Al2–O>	1.890
V3–O2	1.6256(18)				
V3–O9	1.7873(17)				
V3–O10	1.8305(17)				
V3–O13	1.9870(17)				
V3–O12	2.0489(16)				
V3–O14	2.2307(16)				
<V3–O>	1.918				

550
551
552
553

554 Table 4. Proposed hydrogen–bonding for protocaseyite.
555

O_D	H	O_A	O_D–O_A (Å)	H···O_A (Å)	O_D–H–O_A (°)	H–O_D–H (°)
OH1	H1	O13	2.823(2)	1.850(6)	172(4)	
OH2	H2	O9	2.904(2)	1.932(6)	172(4)	
OH3	H3	O1	2.815(2)	2.02(3)	136(3)	
		O1	2.768(2)	2.06(3)	128(3)	
OW1	H4	O8	2.668(2)	1.689(4)	176(4)	
	H5	O6	2.724(2)	1.758(9)	168(4)	110(3)
OW2	H6	O2	2.865(3)	1.906(11)	165(4)	
	H7	OW8	2.736(3)	1.831(19)	152(4)	106(3)
OW3	H8	OW8	2.764(3)	1.823(14)	160(3)	
	H9	O7	2.617(2)	1.661(11)	164(4)	113(3)
OW4	H10	O2	2.790(3)	1.833(11)	164(4)	
	H11	OW10	2.624(3)	1.647(5)	174(4)	102(3)
OW5	H12	O11	2.709(2)	1.729(3)	178(4)	
	H13	OW9	2.644(3)	1.680(10)	167(4)	106(3)
OW6	H14	O12	2.683(2)	1.711(7)	170(4)	
	H15	OW7	2.735(3)	1.823(18)	153(4)	108(3)
OW7	H16	O10	2.752(3)	1.802(16)	162(5)	
	H17	O9	3.254(3)	2.47(4)	136(4)	104(4)
		O10	2.935(3)	2.20(4)	131(4)	
		O11	3.224(3)	2.35(3)	148(4)	
OW8	H18	OW9	2.804(3)	1.88(2)	156(5)	
	H19	O5	3.089(3)	2.18(2)	154(4)	107(4)
OW9	H20	OW7	2.705(3)	1.742(13)	167(5)	
	H21	O2	3.320(3)	2.50(3)	141(4)	111(4)
OW10	H22	O8	3.377(3)	2.49(3)	150(4)	
	H22	O11	3.150(3)	2.33(3)	141(4)	
	H23	OW3	3.015(3)	2.049(11)	168(5)	121(4)

556
557

Table 5. Bond-valence analysis for protocaseyite.

	V1	V2	V3	V4	V5	Al1	Al2	Σ	H1	H2	H3	H4	H5	H6	H7	H8	H9	H10	H11	H12	H13	H14	H15	H16	H17	H18	H19	H20	H21	H22	H23	Σ
O1		1.73						**1.73**			0.10 0.10																					**1.93**
O2			1.62					**1.62**						0.15				0.20											0.10			**2.07**
O3				1.77				**1.77**																								**1.77**
O4					1.79			**1.79**																								**1.79**
O5	1.41			0.49				**1.90**																		0.10					**2.00**
O6	1.30				0.54			**1.84**					0.20																			**2.04**
O7		0.94		0.80				**1.74**									0.25															**1.99**
O8		0.92			0.85			**1.77**				0.20																		0.05		**2.02**
O9			1.04		0.75			**1.79**		0.15															0.03							**1.97**
O10			0.93	0.85				**1.78**																0.20	0.03							**2.01**
O11				0.88	0.88			**1.76**												0.20					0.03					0.05		**2.04**
O12	0.73	0.60	0.51					**1.84**														0.20										**2.04**
O13	0.70	0.58	0.61					**1.89**	0.15																							**2.04**
O14	0.44 0.41	0.30	0.31	0.26	0.22			**1.94**																								**1.94**
OH1						0.57 0.53		**1.10**	0.85																							**1.95**
OH2						0.49	0.57	**1.06**		0.85																						**1.91**
OH3						0.60	0.62	**1.22**			0.80																					**2.02**
OW1						0.45		**0.45**				0.80	0.80																			**2.05**
OW2						0.43		**0.43**						0.85	0.80																	**2.08**
OW3							0.44	**0.44**								0.80	0.75														0.10	**2.09**
OW4							0.50	**0.50**										0.80	0.75													**2.05**
OW5							0.51	**0.51**												0.80	0.75											**2.06**
OW6							0.50	**0.50**														0.80	0.80									**2.10**
OW7								**0.00**															0.20	0.80	0.91			0.20				**2.11**
OW8								**0.00**							0.20	0.20										0.80	0.90					**2.10**
OW9								**0.00**													0.25					0.20		0.80	0.90			**2.15**
OW10								**0.00**											0.25											0.90	0.90	**2.05**
Σ	**4.99**	**5.07**	**5.02**	**5.05**	**5.03**	**3.07**	**3.14**		**1.00**	**1.00**	**1.00**	**1.00**	**1.00**	**1.00**	**1.00**	**1.00**	**1.00**	**1.00**	**1.00**	**1.00**	**1.00**	**1.00**	**1.00**	**1.00**	**1.00**	**1.00**	**1.00**	**1.00**	**1.00**	**1.00**	**1.00**	

Bond-valence parameters for V^{5+}-O are from Brown and Altermatt (1985) and those for Al-O are from Gagné and Hawthorne (2015).
Hydrogen-bond contributions estimated from $O_D \ldots O_A$ distances using Brown and Altermatt (1985).

Figure 1

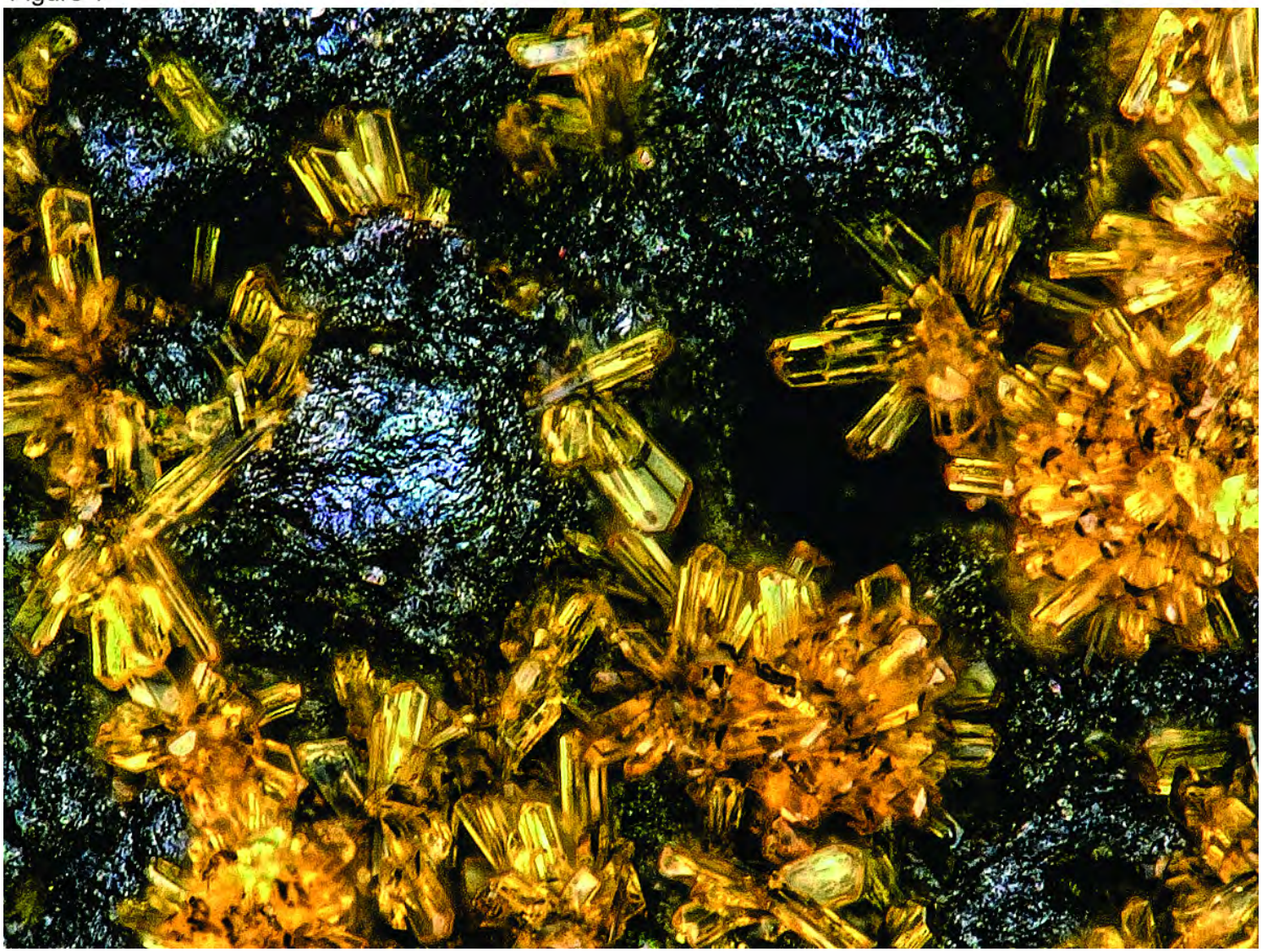

Figure 2

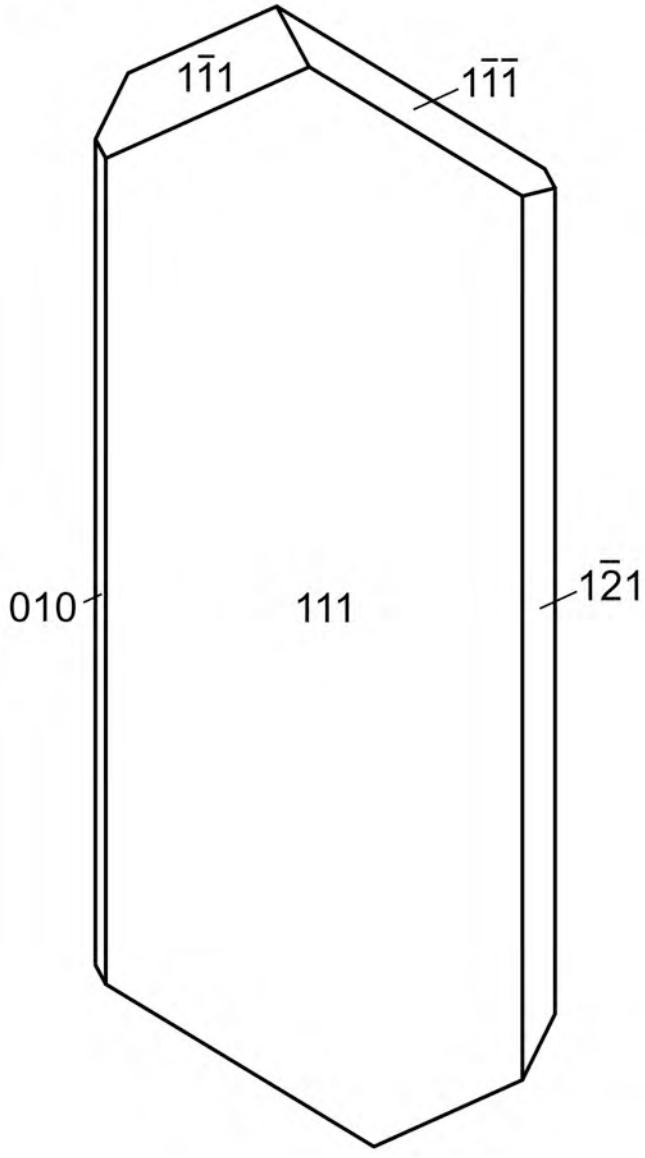

Figure 3

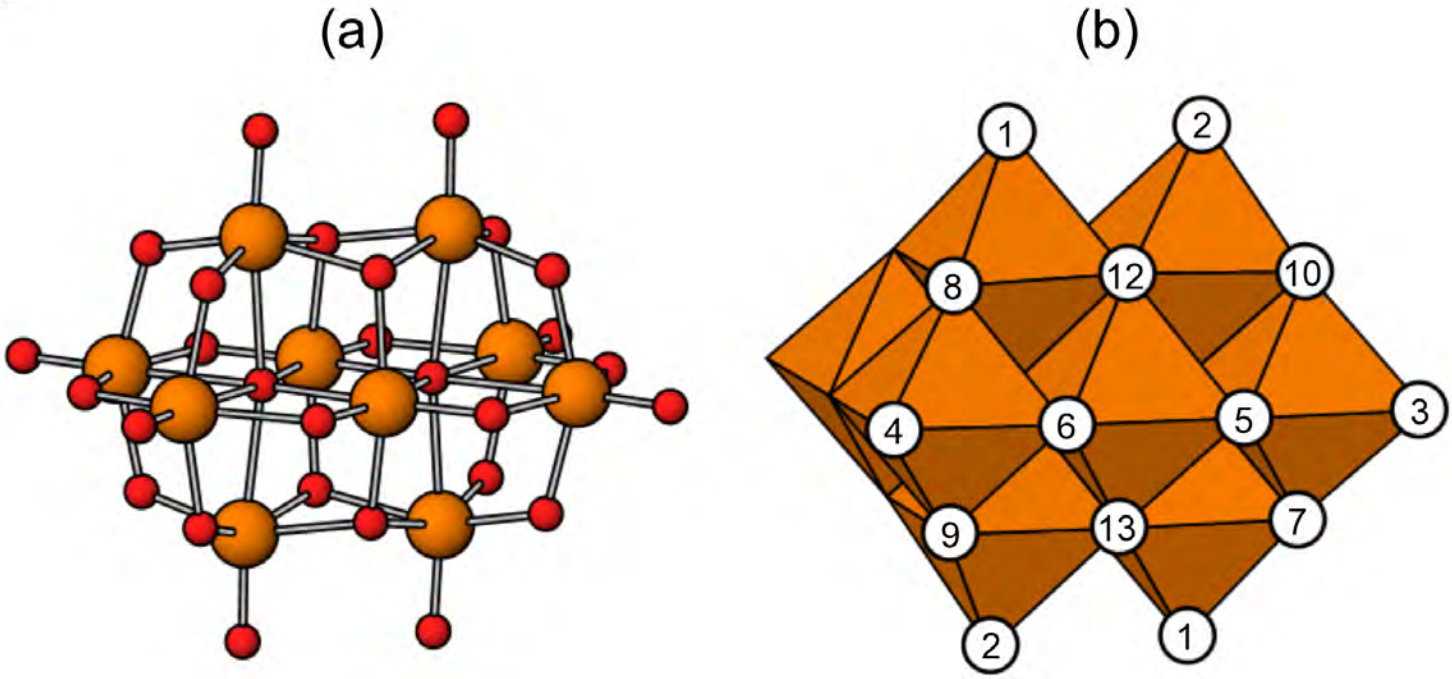

Figure 4

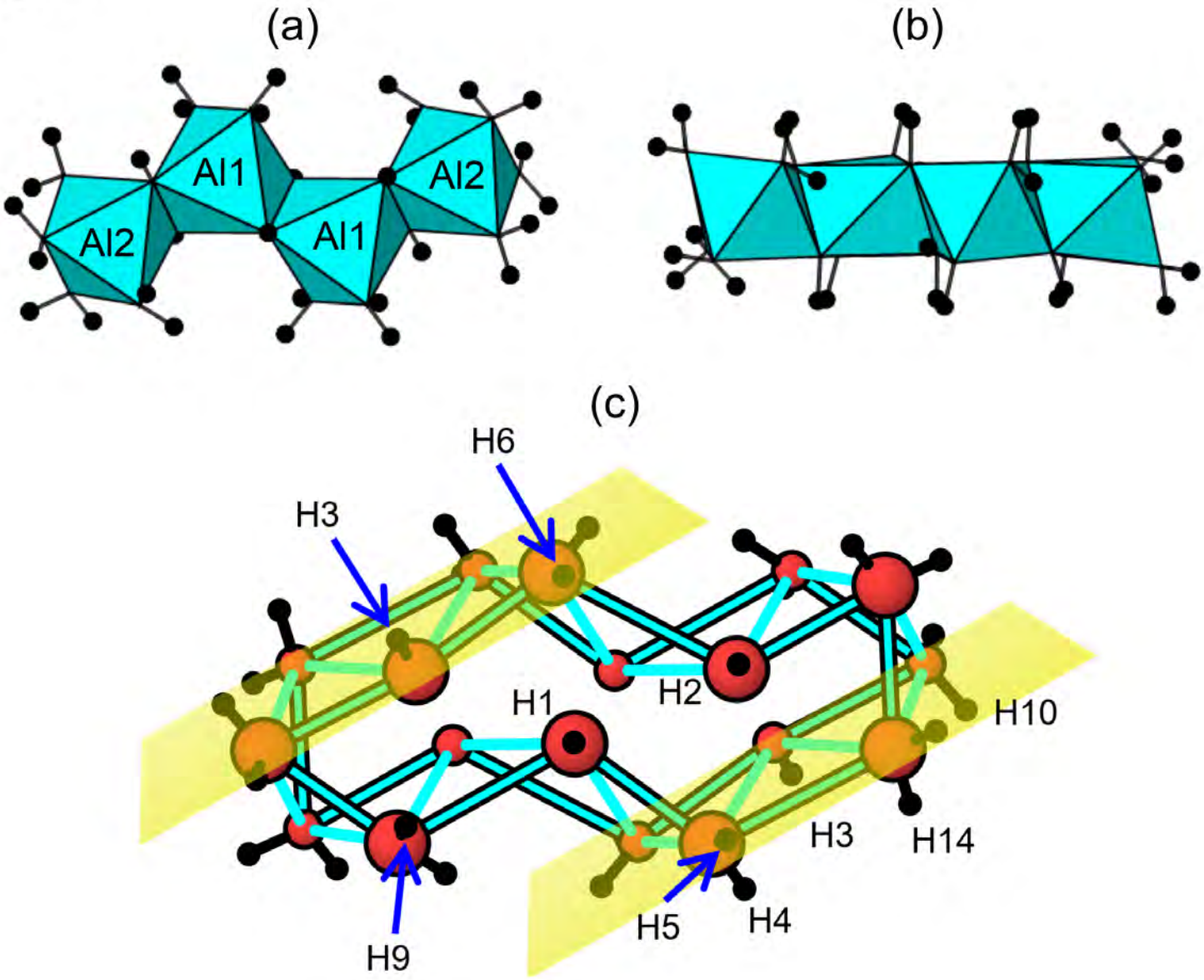

Figure 5

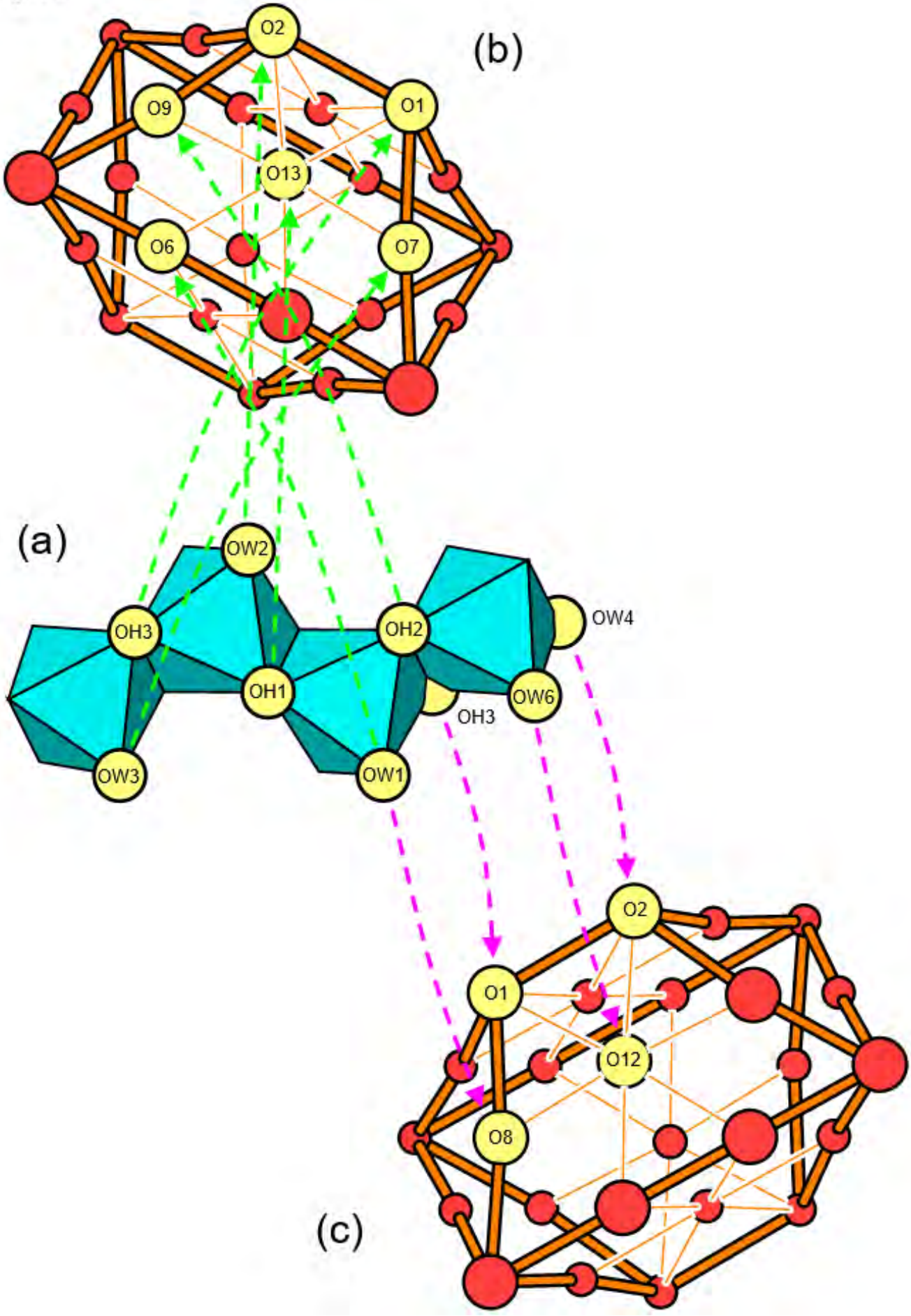
(b)
O2
O9
O1
O13
O6
O7
(a)
OW2
OH3
OH2
OW4
OH1
OW6
OH3
OW3
OW1
(c)
O2
O1
O12
O8

Figure 6

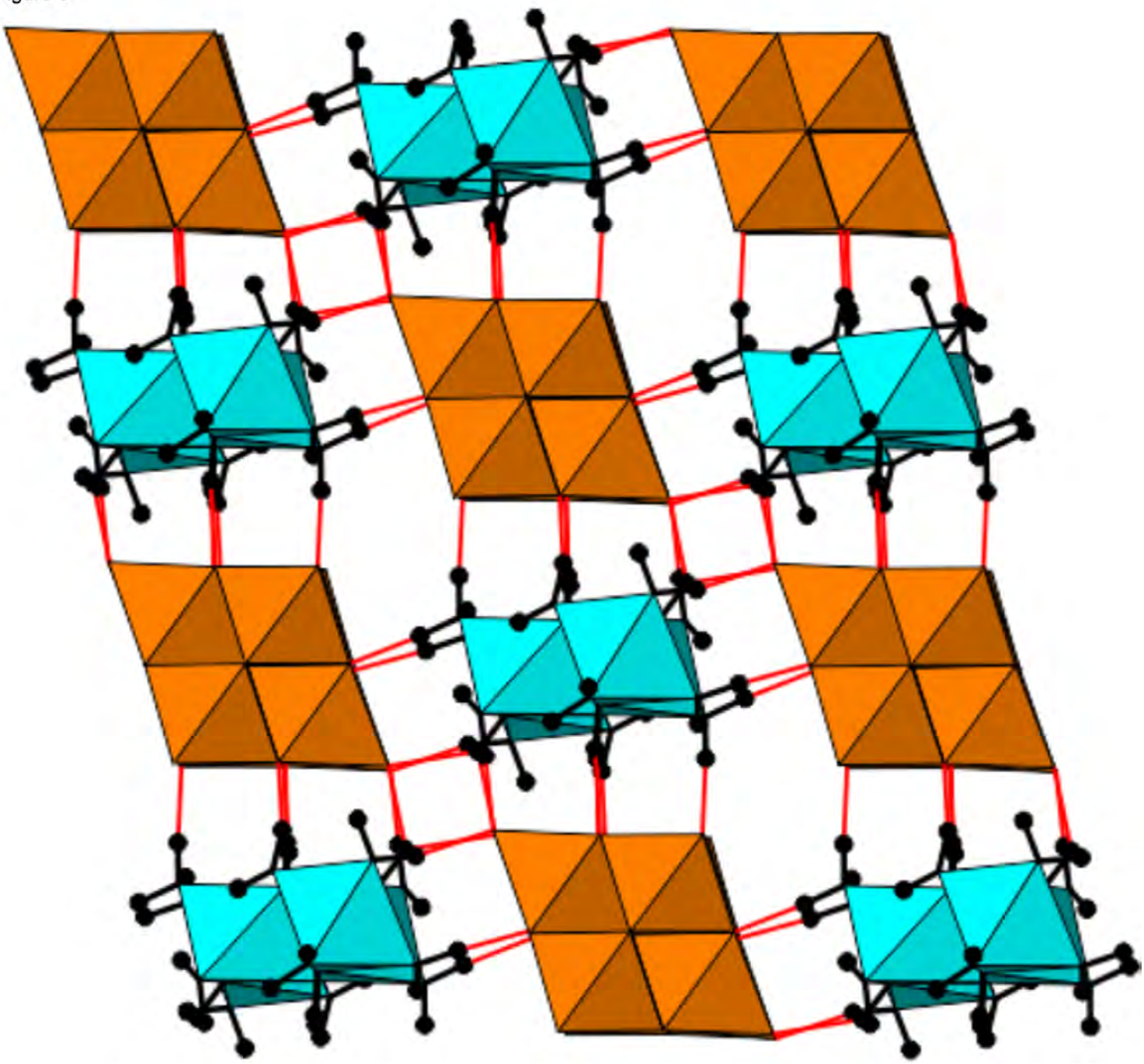

Figure 7

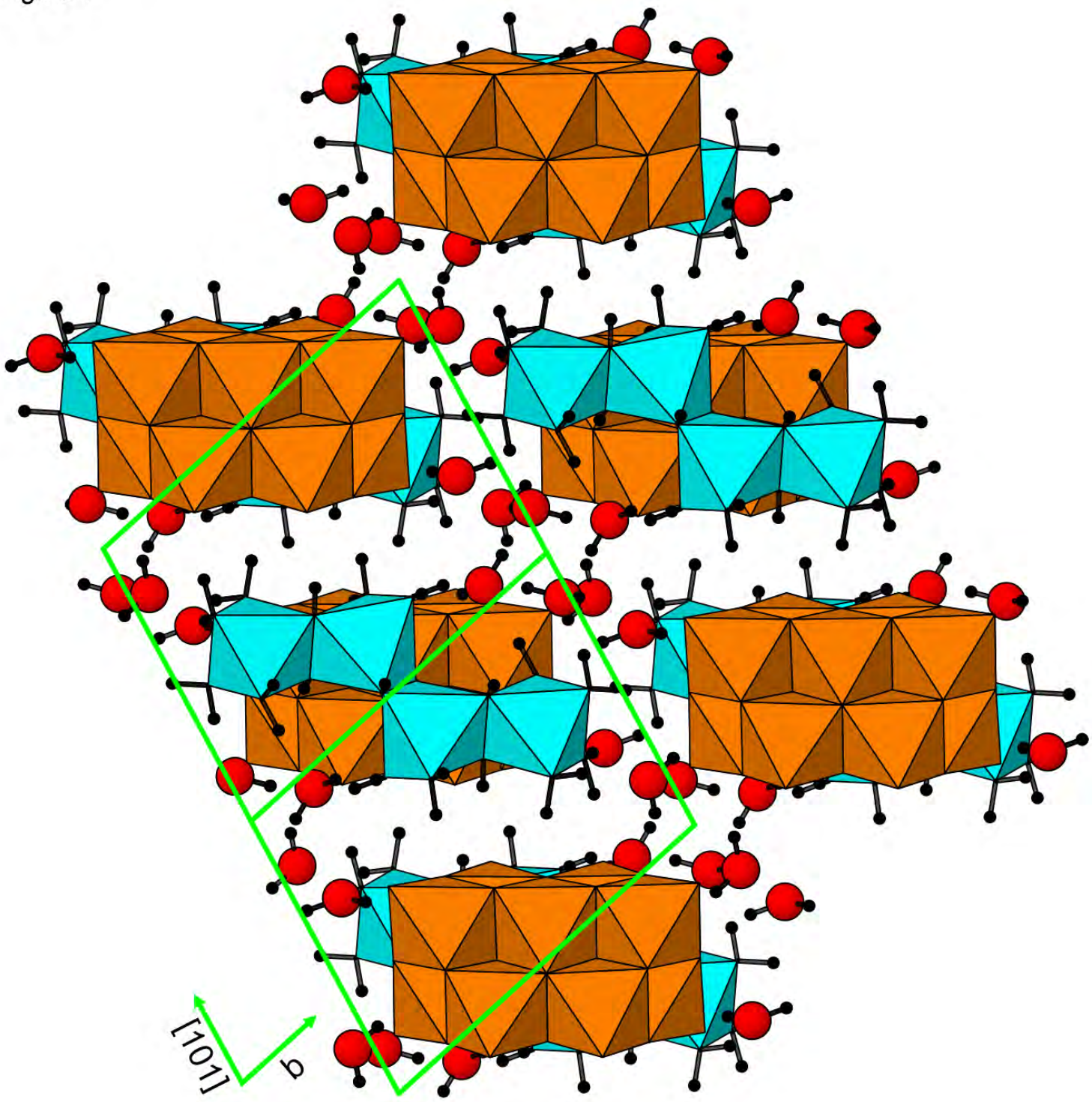

Figure 8

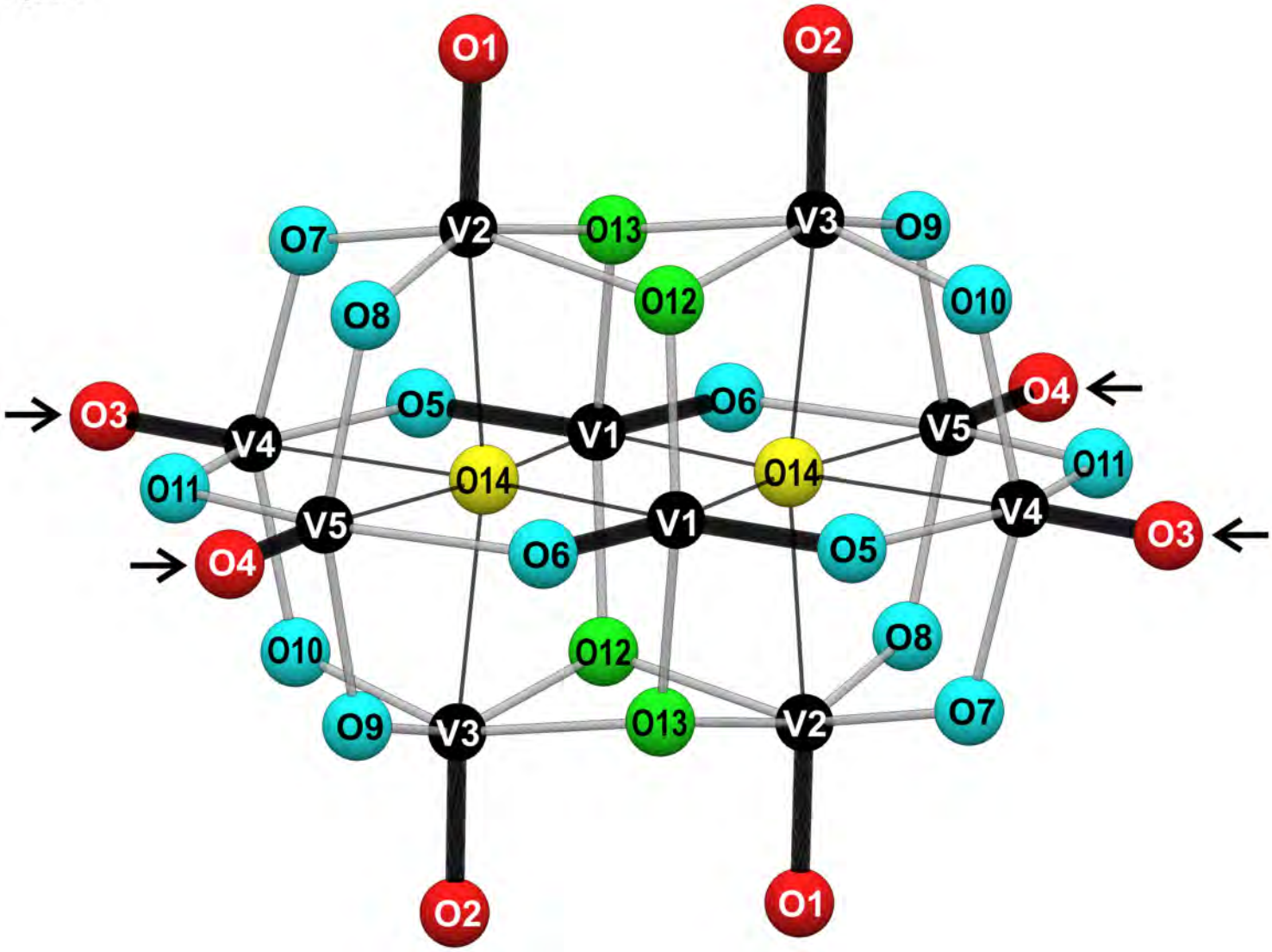
O1
O2
V2
O13
V3
O7
O9
O8
O12
O10
O3
O5
V1
O6
V5
O4
V4
O11
O14
O14
O11
V5
V1
V4
O4
O6
O5
O3
O10
O12
O8
O9
V3
O13
V2
O7
O2
O1

Figure 9